Binding Kinetics of Calbindin-D_{28k} Determined by Flash Photolysis of Caged Ca^{2+}

U. Valentin Nägerl,* David Novo,† Istvan Mody,† and Julio L. Vergara†
†Departments of Physiology and Neurology and *IDP Neuroscience, UCLA School of Medicine, Los Angeles, California 90095 USA

ABSTRACT We have used UV flash photolysis of DM-nitrophen in combination with model-based analysis of Oregon Green 488 BAPTA-5N fluorescence transients to study the kinetics of Ca^{2+} binding to calbindin-D_{28K}. The experiments used saturated DM-nitrophen at a [Ca^{2+}] of 1.5 μM. Under these conditions, UV laser flashes produced rapid steplike increases in [Ca^{2+}] in the absence of calbindin-D_{28K}, and in its presence the decay of the flash-induced fluorescence was due solely to the Ca^{2+} buffering by the protein. We developed a novel method for kinetic parameter derivation and used the synthetic Ca^{2+} buffer EGTA to confirm its validity. We provide evidence that calbindin-D_{28K} binds Ca^{2+} in at least two distinct kinetic patterns, one arising from high-affinity sites that bind Ca^{2+} with a k_{on} comparable to that of EGTA (i.e., $\sim 1 \times 10^7$ M^{-1} s^{-1}) and another with lower affinity and an approximately eightfold faster k_{on}. In view of the inability of conventional approaches to adequately resolve rapid Ca^{2+} binding kinetics of Ca^{2+} buffers, this method promises to be highly valuable for studying the Ca^{2+} binding properties of other biologically important Ca^{2+} binding proteins.

INTRODUCTION

Calcium signaling in excitable cells is characterized by rapid calcium concentration ([Ca^{2+}]) increases resulting from influx through specialized channels in the cell membrane or release from intracellular stores. The [Ca^{2+}] returns to its resting level via the action of extrusion pumps, Ca^{2+} exchangers, Ca^{2+} binding proteins (CBPs), and other endogenous buffers. [Ca^{2+}] signals can propagate through an entire cell as Ca^{2+} waves (Davis, 1992) or can quickly rise and fall in a spatially restricted manner (Neher, 1998b; DiGregorio et al., 1999) and are thought to be shaped by CBPs (Neher, 1998b; Stern, 1992). To understand the interactions between rapidly changing [Ca^{2+}] levels and CBPs, one must not only know the protein's concentration and equilibrium binding properties (K_d), but also the association and dissociation rate constants (k_{on} and k_{off}, respectively) of the Ca^{2+} binding reaction.

Calbindin-D_{28K} (CB_{28K}) is a prominent member of the EF hand superfamily of CBPs, characterized by the EF hand motif, which permits the specific and reversible binding of Ca^{2+} (Kawasaki et al., 1998). CB_{28k} is found in specific central nervous system (CNS) neurons (Celio, 1990) such as cerebellar Purkinje cells and hippocampal granule cells, where it is thought to be present in high cytosolic concentrations (up to hundreds of micromolar) (Fierro and Llano, 1996; Baimbridge, 1992). Thus far CB_{28K} has not been found to play a role in Ca^{2+}-dependent regulation of enzymatic activity comparable to that of calmodulin (Kennedy, 1989). However, in view of its ability to bind four Ca^{2+} ions per molecule (Veenstra et al., 1997) with physiologically relevant affinity (Cheung et al., 1993; Gross et al., 1993), it is expected to play a major role as an intracellular Ca^{2+} buffer. Indeed, data from CB_{28k} knock-out mice experiments are consistent with such a role (Airaksinen et al., 1997; Klapstein et al., 1998; Pasti et al., 1999). Furthermore, CB_{28k} was shown to limit the Ca^{2+}-dependent inactivation of Ca^{2+} currents in hippocampal granule cells (Nägerl et al., 2000), presumably by competing for Ca^{2+} with the Ca^{2+} sensor responsible for inactivation.

Little is known about the Ca^{2+} binding kinetics of CPBs, including CB_{28K}. This is mainly due to technical limitations involved in measuring association rate constants of diffusion-limited reactions (Eigen, 1963). A commonly used technique for these purposes is stopped flow, which has previously been used to investigate the Ca^{2+} binding kinetics of CPBs other than CB_{28k}, such as synaptotagmin (Davis et al., 1999), calmodulin (Bayley et al., 1984), and calbindin-D_{9k} (CB_{9K}) (Martin et al., 1990). A major limitation of the stopped-flow method is its inherent dead time in the range between 1 and 2 ms (Czerlinski, 1966). To accurately determine kinetic rate constants we must have information on both the amplitude and shape of the Ca^{2+} signals during the initial phases of the reaction, which can occur during the dead time of the technique. This limitation is especially evident when one measures Ca^{2+} association rate constants of polypeptides such as the C2A domain of synaptotagmin, where the entire reaction was completed within the dead time of the instrument and only a lower estimate of the k_{on} could be determined (Davis et al., 1999).

The temperature-jump method is another means for tracking fast kinetics, which has been used to characterize the Ca^{2+} binding reactions of chelators and dyes (Kao and Tsien, 1988; Naraghi, 1997). Even though this technique has a dead time of only several microseconds, its usefulness is limited by the fact that the kinetic rate constants are inferred from a temperature-jump-induced displacement from equilibrium for multiple Ca^{2+}-binding molecular spe-

Received for publication 14 July 2000 and in final form 31 August 2000.
Address reprint requests to Dr. Valentin Nägerl, Max-Planck Institute of Neurobiology, Am Klopferspitz 18A, 82152 Martinsried, Germany, Tel: 49-89-8578-3718, Fax: 49-89-8995-0037, E-mail: valentin@neuro.mpg.de.

0006-3495/00/12/3009/10 $2.00

cies. The interpretation of the relaxation has only been accomplished assuming either simplifying conditions such as small perturbations in the $[Ca^{2+}]$ (Czerlinski, 1966) or that the relaxation responses are a complicated sum of exponentials (Naraghi, 1997). Neither assumption is necessarily valid under all experimental conditions that one would wish to examine.

Here we report a novel technique to measure the Ca^{2+} binding kinetics of CBPs, such as CB_{28K}, that is based on flash photolysis of DM-nitrophen (DM-n), a caged Ca^{2+} compound. The method was modified from that previously reported (Escobar et al., 1995, 1997), where it was used to investigate the kinetic properties of Ca^{2+} indicator dyes. Several changes were made to accurately determine the Ca^{2+} binding properties of nonfluorescent Ca^{2+} buffers: 1) The free $[Ca^{2+}]$ was monitored using OGB-5N, a low-affinity Ca^{2+} indicator with binding kinetics faster than those of any of the buffers studied. 2) A relatively high preflash free $[Ca^{2+}]$ was used to generate a steplike $[Ca^{2+}]$ driving function, fast enough (<200 μs rise time) to resolve rapid Ca^{2+} binding kinetics. 3) Mathematical model simulations, which incorporated the Ca^{2+}-binding reactions of all of the species in the solution, were fitted to the experimental data to extract kinetic parameters. The dead time associated with this flash photolysis method is as low as 10 μs (Escobar et al., 1997), thus allowing us to clearly resolve the rising phase and amplitude of fast Ca^{2+} signals after laser pulse delivery.

We first confirmed the validity of this technique by using EGTA, a well-characterized Ca^{2+} buffer (Naraghi, 1997; Smith et al., 1984; McGuigan et al., 1991; DiGregorio et al., 1998, 1999). We then used it to study Ca^{2+} binding to CB_{28K}. Our results show that CB_{28K} possesses two kinetically distinct types of Ca^{2+} binding sites.

The methodology described here should have broad applicability for the study of the Ca^{2+} binding properties of a wide array of CBPs, which should be useful for understanding biological processes such as synaptic transmission (Adler et al., 1991; Atluri and Regehr, 1996; Chen and Regehr, 1999) and muscle excitation-contraction coupling (Vergara and Delay, 1985; Hollingworth et al., 1996), in which Ca^{2+} buffering is thought to play a key role.

MATERIALS AND METHODS

Optical set-up

As described previously (Escobar et al., 1997), the experimental setup consisted of a spot detection system and a fiber optic system to deliver flashes of UV light to sample droplets (flash solution) placed on an experimental chamber situated in the field of view of an inverted fluorescence microscope (model IM; Zeiss, Oberkochen, Germany). Epifluorescence illumination was supplied by an argon laser (488 nm, model 95; Lexel, Freemont, CA) operated at power output levels between 45 and 90 mW. The laser beam was spatially filtered with a Gaussian filter (15-μm-diameter pinhole) and then focused onto the epifluorescence illumination port of the microscope. A dichroic mirror, with a central wavelength of 510 nm, and a 515-nm emission filter (Melles Griot, Carlsbad, CA) were used for proper wavelength selection. A 40× objective (M Plan40; Nikon, Tokyo, Japan) was used to form the image of the pinhole (illumination spot) and to collect the fluorescence. The effective illumination spot measured 1.3 μm in diameter.

UV flash delivery

Flashes of UV light (347 nm for 20 ns) were generated by a frequency-doubled ruby laser (Lumonics, Rugby, UK) and guided through a cladded fused-silica fiber optic (diameter 200 μm). With a micropositioner, the fiber optic was centered relative to the illumination spot, its tip touching the coverslip of the experimental chamber, and fully immersed in a 20-μl flash solution droplet. The energy of each UV flash was measured with a peak detection circuit located in the laser head, the output of which was acquired simultaneously with the fluorescence traces and calibrated with a digital bolometer (model 36-5002T2; Scientech, Boulder, CO).

Fluorescence recording

OGB-5N (Molecular Probes, Eugene, OR) fluorescence was measured with an ultralow capacitance PIN photodiode (HR-005; United Detector Technologies, Culver City, CA), using the integrating headstage of a patch-clamp amplifier (Axopatch 200A; Axon Instruments, Foster City, CA) as a current-to-voltage converter. The analog signal was filtered with an 8-pole low-pass Bessel filter with a cut-off frequency set at 2 kHz and digitized at 50 kHz (PCI-MIO-16XE-10; National Instruments, Austin, TX). Although the excitation spectrum of OGB-5N peaks at 494 nm, the high energy of the UV flash still induced a large and brief fluorescence transient, which would have saturated the detection system. To avoid this artifact, the integrating capacitor of the Axopatch headstage was short-circuited for 50 μs, encompassing the point of UV flash delivery, to prevent the amplifier from saturating and to allow faithful recording of the rising phase of fluorescence transients immediately after flash delivery. Data acquisition and timing were controlled by custom-written software in G-language (LabVIEW; National Instruments). Flash generation, shutter control, and capacitor blanking were timed with a Digitimer D4030 (Hertfordshire, England).

All fluorescence traces were expressed as

$$\frac{\Delta F}{F} = \frac{F(t) - F_{\text{rest}}}{F_{\text{rest}}} \tag{1}$$

where $F(t)$ is the acquired fluorescence record and F_{rest} is the resting fluorescence before flash delivery. The data were imported into Origin (Microcal, Northampton, MA) for exponential time constant fitting using a nonlinear least-squares algorithm. Steady-state $\Delta F/F$ values were converted into absolute $[Ca^{2+}]$, using the following equilibrium formula (Vergara and DiFranco, 1992; Escobar et al., 1997):

$$[Ca^{2+}] = K_d\left(\frac{F/F_{\max} - 1/F_{\text{ratio}}}{1 - F/F_{\max}}\right) \tag{2}$$

where K_d is the equilibrium dissociation constant of OGB-5N, $F_{\max}$ is the maximum fluorescence, F_{ratio} is the ratio of the maximum and minimum fluorescence, and F is the steady-state fluorescence. $F_{\max}$ was measured by raising the $[Ca^{2+}]$ in the flash solution to 5 mM.

Ca^{2+} electrode measurements

The $[Ca^{2+}]$ of all solutions was measured with custom-made Ca^{2+} electrodes (Baudet et al., 1994). Glass pipettes (BF-160-80-10; Sutter Instrument, Novato, CA) were fire-polished, silenized, and filled by capillary

action with a Ca^{2+}-selective ionophore (Cocktail A; Fluka, Milwaukee, WI) mixed at equal volume with 1% polyvinylchloride PVC dissolved in tetrahydrofuran (THF). A thin membrane was formed after evaporation of the THF, and the electrodes were stored at room temperature for at least 2 days before use. NaCl-based pCa standard solutions (290 mOsm, Calbuf-2; WPI, New Haven, CT) were used for calibration. The pCa 6 standard was used as the intrapipette reference solution. The voltage offsets were zeroed when the electrode was submerged in the pCa 6 solution. Electrodes were used only if they exhibited linearity (>26.5 mV/decade) in the pCa range from 3 to 7.4 and suffered less than 1 mV/h drift. The voltage offset in the pCa electrode reading due to the salt mismatch between the NaCl-based Ca^{2+} calibration and the KCl-based flash solutions was measured as a function of the $[Ca^{2+}]$ and corrected. In the Scatchard EGTA experiments, NaCl was used in the buffer solution to avoid complications associated with variable offsets at low $[Ca^{2+}]$.

Preparation of solutions

All flash solutions contained (in mM) 120 KCl, 40 HEPES, 5 DM-n, and 0.1 OGB-5N. Osmolarity and pH were set at 280 mOsm and 7.3, respectively. They also included either variable concentrations (0, 0.25, 0.5, 1, and 2 mM) of EGTA (Sigma, St. Louis, MO) or 700 μg of lyophilized recombinant CB_{28k} (courtesy of Dr. K. G. Baimbridge, University of British Columbia) per 200 μl of solution (125 μM). The $[Ca^{2+}]$ of the flash solutions was titrated to 1.5 μM with $CaCl_2$. A 20-μl droplet of flash solution was placed on the coverslip, fully enclosing the tip of the fiber optic. Because the fraction of the droplet volume exposed to the flash was small, we were able to acquire ~10 flash-evoked transients from single droplets without significant changes in the baseline conditions. All experiments were conducted at room temperature (20–22°C).

Scatchard analysis of Ca^{2+} equilibrium binding to EGTA

The effective equilibrium dissociation constant (K_d) of EGTA was measured by titration, using the Ca^{2+} electrode, and calculated from Scatchard plots according to procedures described elsewhere (Bers, 1982; DiPolo et al., 1983). The solution volume of 10 ml was mixed intermittently with a magnetic stir bar when $CaCl_2$ from stock solutions (1 M, 100 mM, 25 mM, 5 mM) was introduced via a calibrated pipette. For comparison, we also calculated K_d values for EGTA, using the MaxChelator simulation package (Bers et al., 1994).

Data analysis and kinetic parameter extraction

A general-purpose differential equation solver (Berkeley Madonna 8.0, UC Berkeley) was used for model fitting and parameter extraction, in which a downhill simplex optimization algorithm minimized the root-mean-square (RMS) value between model predictions and experimental data traces. The model simulated UV flash-induced $\Delta F/F$ fluorescence transients in the presence of a known concentration of a Ca^{2+} buffer according to the scheme shown in Fig. 1. The dynamic redistribution of Ca^{2+} among the three Ca^{2+}-binding species (DM-n, OGB-5N, and the Ca^{2+} buffer under investigation) was modeled after a rapid (τ = 20 μs) and drastic (>600,000-fold) increase in the dissociation rate constant of DM-n (Ellis-Davies and Kaplan, 1994; Escobar et al., 1997) (see Appendix for details), which effectively liberated and acted as the source for Ca^{2+}. The kinetic and fluorescent properties of OGB-5N and DM-n used in the model were taken from the literature or were independently verified in our laboratory (see Appendix for details). To match the signal conditioning of modeled data with that of the experimental traces, the output of the model was digitally filtered. For computational efficiency we implemented a single time constant filter (τ = 80 μs) that approximated the analog Bessel filter. The

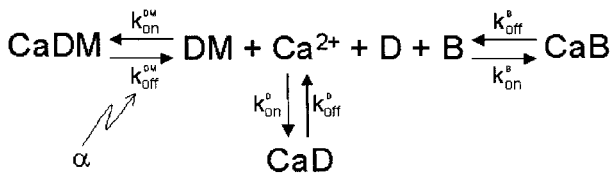

FIGURE 1 Scheme of the model used to simulate the dynamic redistribution of Ca^{2+} generated by flash photolysis of DM-n. CaDM, CaD, and CaB represent the concentration of Ca^{2+} bound to DM-n, dye, or buffer, respectively. Ca^{2+}, D, and B are the free concentrations of Ca^{2+}, dye, and buffer, respectively. α models the fraction of Ca^{2+}-bound DMn that is photolyzed by the UV laser flash.

filtered model simulations were fitted to the normalized fluorescence transients using α (flash energy), k_{on}, and K_d as the only floating parameters. Up to five $\Delta F/F$ traces obtained from the same droplet but at different flash energies (i.e., $[Ca^{2+}]$ step size) were fitted simultaneously by forcing the values of k_{on} and K_d to be identical (for any family of simulated $\Delta F/F$ transients) and allowing only the α parameter to vary within.

RESULTS

Photolysis of DM-n generates steps in free $[Ca^{2+}]$

A previous paper has described in detail the dynamic properties of Ca^{2+} spikes induced by DM-n flash photolysis and their dependence on the experimental conditions, namely the resting $[Ca^{2+}]$ and the UV flash energy (Escobar et al., 1997). It was suggested that at relatively high preflash $[Ca^{2+}]$, flash photolysis generates Ca^{2+} steps because under these conditions DM-n is saturated and any rebinding of Ca^{2+} to free DM-n becomes negligible. Fig. 2 shows that when the resting $[Ca^{2+}]$ was titrated to 1.5 μM, in the absence of EGTA or CBPs, we were able to induce steplike changes in $[Ca^{2+}]$. These were evidenced by rapid increases in OGB-5N fluorescence (200 μs, 10–90% rise time), the

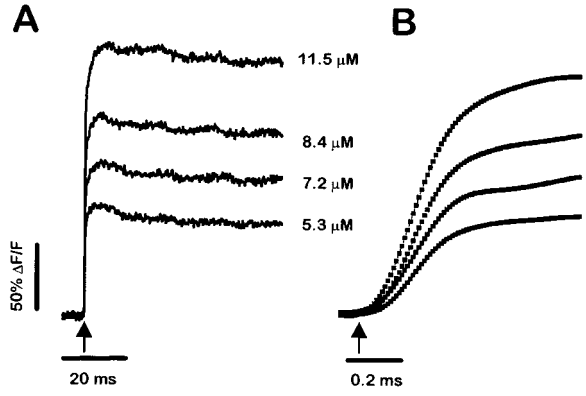

FIGURE 2 UV flash photolysis of DM-n produces steplike changes in $[Ca^{2+}]$. (*A*) OGB-5N fluorescence increases in response to UV laser flashes (delivered at the *arrow*) of six different energies. The measured relative energies (*from bottom to top trace*) were 1.00, 1.20, 1.44, and 1.57. The absolute $[Ca^{2+}]$ plateau values (10 ms after flash delivery) were calculated as described in Materials and Methods and are shown on the right-hand side of each trace. (*B*) As in *A*, but on an expanded time scale.

amplitude of which depended on the flash energy (Fig. 2). The decay of these fluorescence signals was constrained to within <8% in 60 ms and ~5% in 20 ms (Fig. 2 *A*), demonstrating only a moderate [Ca^{2+}] decrease (either by diffusion out of the detection volume or rebinding to residual DM-n) on the time scale of Ca^{2+} buffering we sought to study. Fig. 2 *B* shows, on an expanded time scale, that flash artifacts do not compromise the onset of the fluorescence signal.

Ca^{2+} association with EGTA

To test the validity of using UV flash photolysis to accurately estimate the kinetic Ca^{2+} binding properties of nonfluorescent Ca^{2+} buffers, we chose to study the well-known synthetic Ca^{2+} buffer EGTA, because it is available in high purity (>97%) and it binds Ca^{2+} with simple 1:1 stoichiometry (Bers et al., 1994). Moreover, the kinetic properties of this buffer have been studied (Smith et al., 1984; Naraghi, 1997; DiGregorio and Vergara, 1997).

Scatchard analysis of EGTA equilibrium binding of Ca^{2+}

Because the affinity of EGTA for Ca^{2+} is strongly influenced by parameters such as ionic strength and pH (Bers, 1982; Bers et al., 1994), we determined its effective equilibrium dissociation constant (K_d) by Scatchard analysis of our experimental solutions. Fig. 3 *A* shows linear regressions of the titration data obtained with Ca^{2+}-sensitive electrodes. The filled symbols represent uncorrected data, yielding a K_d of 72 ± 4 nM ($n = 3$) and a total [EGTA] of 920 μM. We chose to correct the data by assuming that the *total* [EGTA] in the solution was exactly 1 mM, which implied a total Ca^{2+} contamination of 80 μmol/liter. The order of magnitude of this contamination is consistent with the specified maximum Ca^{2+} levels inherent in the stock compounds. The corrected values were replotted (*open symbols* in Fig. 3 *A*), and the K_d obtained from the linear fit to the corrected data was 68 ± 3.5 nM ($n = 3$). However, multiple linear regression analysis revealed that the two K_d values were not statistically different ($p > 0.2$).

Single time constant fitting approach

Fig. 3 *B* shows the exponential decay of flash-induced OGB-5N fluorescence transients in the presence of variable concentrations of EGTA (0.25, 0.5, 1, and 2 mM). The addition of EGTA to the flash solution led to the appearance of a decay phase in the transients, which became more rapid and pronounced as the concentration of EGTA was increased from 0 to 2 mM. Because the relaxation of the fluorescence transients could be well fitted by single exponentials (*smooth lines* in Fig. 3 *B*), one might be tempted to directly derive the kinetic rate constants from these time

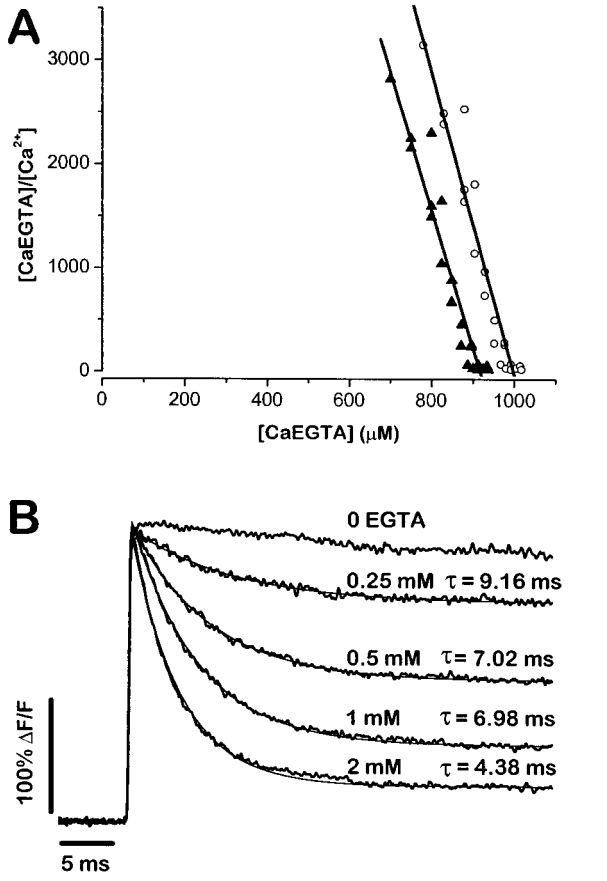

FIGURE 3 (*A*) Scatchard plot to determine the effective Ca^{2+} dissociation constant (K_d) of EGTA. The ordinate represents the ratio of the concentration of bound [Ca^{2+}] over free [Ca^{2+}], and the abscissa is the bound [Ca^{2+}] as calculated from Ca^{2+} electrode data. The straight line is a linear least-squares (regression) fit to the data points. The open circles show the same data set corrected for 80 μmole/liter Ca^{2+} contamination, which was found to shift the *x* axis intercept of the regression line to 1 mM. (*B*) Dependence of the decay in $\Delta F/F$ transients on the [EGTA]. Thin lines represent fits to the data (fit function: $A \times \exp(-t/\tau) + C$, where A is amplitude, C is steady-state offset, and τ is a time constant) and are superimposed on the individual data traces (*thick lines*). The values of total [EGTA] and τ are shown above each trace.

constants. If the only Ca^{2+} binding reaction occurring in the droplet involved EGTA, it would obey the simple scheme

$$[Ca^{2+}] + [EGTA] \underset{k_{off}}{\overset{k_{on}}{\leftrightharpoons}} [CaEGTA] \tag{3}$$

Under these circumstances, the [Ca^{2+}] response to a small step in *total* [Ca^{2+}], relative to the *total* [EGTA], would be an initial jump followed by an exponential decay with the time constant

$$\tau = (k_{on} \times [EGTA] + k_{off})^{-1} \tag{4}$$

Nevertheless, this simple kinetic analysis is inappropriate under our experimental conditions for the following reasons. First, the single-buffer assumption is invalid, because

the Ca^{2+} indicator itself represented a significant buffer in the flash solution. Second, the amount of uncaged Ca^{2+} was comparable to the [EGTA], as evidenced by the fact that the fluorescence signal does not decay back to its preflash value. Third, the OGB-5N fluorescence transient is a low-pass filtered representation of the [Ca^{2+}] (Escobar et al., 1997). For these reasons, we decided to analyze the flash photolysis data, using the comprehensive model outlined in Fig. 1 and developed in the Appendix, which accurately represents the experimental conditions.

Association rate of EGTA: full model fitting approach

Fig. 4 shows families of flash-induced OGB-5N fluorescence transients (*thick traces*) obtained with different concentrations of EGTA (0.25, 1, and 2 mM). At each [EGTA], four $\Delta F/F$ traces were obtained at different flash energies. They were fitted simultaneously, assuming the single binding scheme of Eq. 3, by forcing the values of k_{on} and K_d to be identical for each family of simulated traces at a given EGTA concentration, and only allowing the α parameter of the model (see Appendix for details) to vary within the family. The resulting best-fit simulations (*thin traces*) are shown superimposed on the data traces in Fig. 4. As expected, regardless of the EGTA concentration used, the values of k_{on} and K_d were similar, ranging from 0.93×10^7 to 1.3×10^7 M^{-1} s^{-1} for k_{on}, and from 64 to 83 nM for K_d.

The pooled EGTA K_d value obtained from kinetic modeling, shown in Table 1, is in close agreement with that obtained from Scatchard analysis. Furthermore, it is consistent with the range calculated using the MaxChelator program, which predicts a K_d of 101 nM at pH 7.3 and 64 nM at pH 7.4 and 22°C.

Kinetic properties of CB_{28k}

Having established the validity of model-based fitting of Ca^{2+} flash photolysis data to determine the kinetic rate constants of a nonfluorescent Ca^{2+} buffer, we used this method to study the kinetics of Ca^{2+} binding to CB_{28k}. As in the EGTA flash experiments, we titrated the [Ca^{2+}] of the protein sample solutions to 1.5 μM. Fig. 5 *A* shows a family of five $\Delta F/F$ transients (*thick traces*) elicited by UV flashes of varying energy in the presence of 125 μM CB_{28k}. In an attempt to derive values for k_{on} and K_d, we proceeded to fit a *uniform* binding site model, which takes into account the four Ca^{2+} binding sites per molecule reported for CB_{28k} (Veenstra et al., 1997) but assumes that they are kinetically identical. Up to five transients were fitted simultaneously as described for EGTA (Fig. 5 *A, thin traces*). However, this model fails to adequately fit both the amplitude and time course of the fluorescence transients. This is particularly evident at early times (0.5–2 ms), as illustrated in the lower panel of Fig. 5 *A* on an expanded time scale.

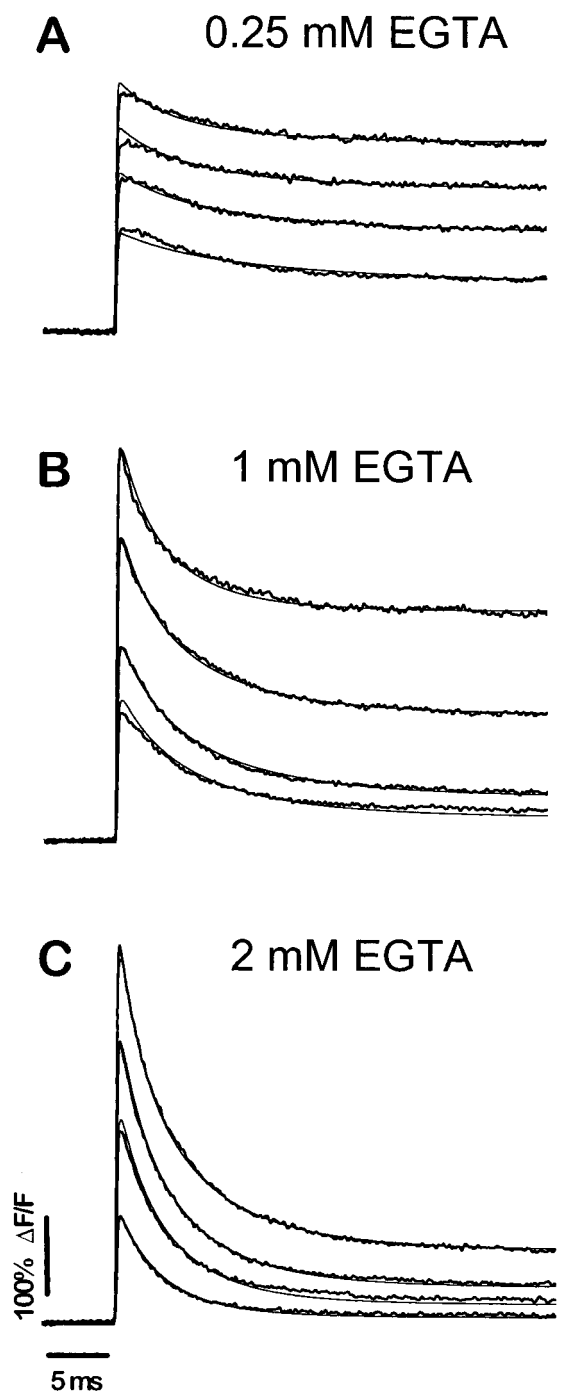

FIGURE 4 Dependence of the decay in $\Delta F/F$ transients on flash energy and [EGTA] and predictions by model simulations. In all panels thick lines represent experimental data and thin lines model simulations. (*A*) 0.25 mM EGTA, $k_{on} = 0.98 \times 10^7$ M^{-1} s^{-1}, $K_d = 66$ nM. α was 2.9, 4.9, 6.4, 8.0×10^{-3}, from the lowest to the highest trace. (*B*) 1 mM EGTA, $k_{on} = 0.99 \times 10^7$ M^{-1} s^{-1}, $K_d = 64$ nM, $\alpha = 4.5, 6.4, 10.8, 14.9 \times 10^{-3}$. (*C*) 2 mM EGTA, $k_{on} = 0.93 \times 10^7$ M^{-1} s^{-1}, $K_d = 64$ nM, $\alpha = 3.5, 7.1, 10.2, 14.1 \times 10^{-3}$.

In view of the inadequacy of this uniform model, we reanalyzed the data with a *heterogeneous* binding site model that incorporated two sets of kinetically distinct Ca^{2+}-bind-

TABLE 1 Kinetic parameters of EGTA and CB_{28k}

Ca^{2+} buffer	K_{d1}	k_{on1}	K_{d2}	k_{on2}
EGTA	71 ± 4 (model fit; n = 5, 19 traces) 68 ± 3.5 (Scatchard; n = 3)	1.05 ± 0.07	NA	NA
CB_{28k} (n = 4, 20 traces)				
(3:1)	175 ± 11	1.3 ± 0.02	513 ± 32	7.7 ± 0.5
(2:2)	237 ± 41	1.1 ± 0.1	411 ± 82	8.7 ± 0.9

Parameter values were obtained from flash photolysis data or Scatchard analysis. Indices 1 and 2 refer to high- and low-affinity sites, respectively. Because the EGTA data were fitted by a single-kinetics model, second site values are not applicable (NA). CB_{28k} data were fitted assuming that the four Ca^{2+} binding sites are distributed in kinetically distinct binding sites with a 3:1 or a 2:2 ratio (high:low affinity). All values represent mean ± SE and are in nM for K_d and $\times 10^7$ M^{-1} s^{-1} for k_{on}.

ing sites stoichiometrically distributed in a 3:1 or a 2:2 ratio. Fig. 5 *B* (*thick lines*) shows the same transients as Fig. 5 *A*, but fitted by this model. The improvement in the fit is striking. Whereas the uniform model consistently underestimated the peak and initial decay of the $\Delta F/F$ traces, the heterogeneous model closely predicted the peak and overall

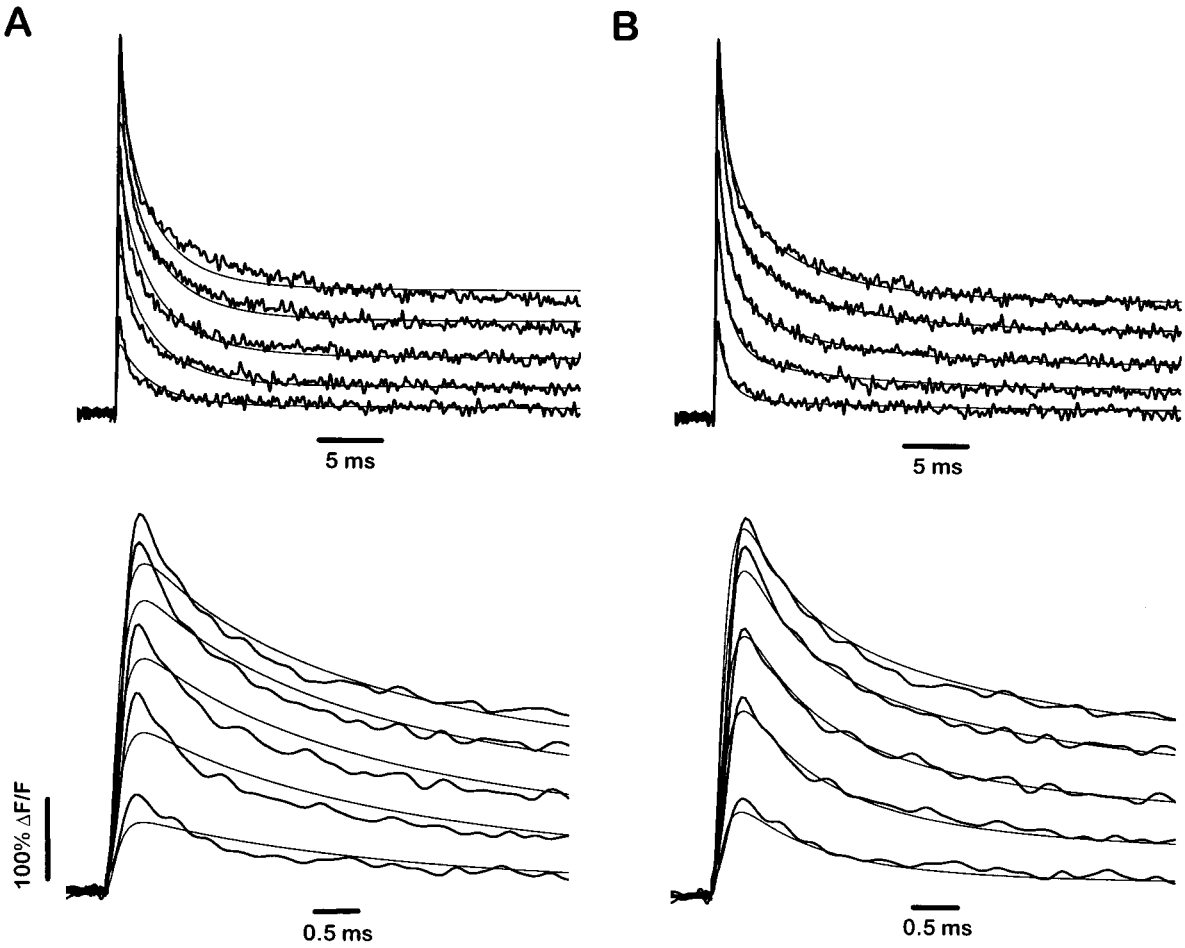

FIGURE 5 UV flash-induced $\Delta F/F$ transients in the presence of 125 μM CB_{28k}. The upper panels show the decay of a family of experimental $\Delta F/F$ transients (*thick traces*) elicited by UV flashes of varying energy and associated model simulations (*thin traces*), and the lower panels show the same traces on an expanded (10×) time scale. *A* and *B* show the same experimental traces. (*A*) The best-fit simulations are based on 500 μmol/liter of Ca^{2+}-binding sites with a uniform binding scheme. $k_{on} = 2.37 \times 10^7$ M^{-1} s^{-1}, K_d = 158 nM. The α's were 2.1, 4.9, 7.4, 9.4, and 10.8×10^{-3}, from the lowest to the highest trace. (*B*) The simulations are based on a heterogeneous binding site model with 375 μM high-affinity and 125 μM low-affinity binding sites (3:1 stoichiometry). For the high-affinity site, $k_{on1} = 1.30 \times 10^7$ M^{-1} s^{-1}, K_{d1} = 185 nM. For the low-affinity site, $k_{on2} = 8.53 \times 10^7$ M^{-1} s^{-1}, K_{d2} = 521 nM. The α's were 2.9, 6.5, 9.6, 12.3, and 14.1×10^{-3}, from the lowest to the highest trace.

time course of the transients. This improvement is quantitatively reflected by a factor of 2 decrease in the RMS value. Moreover, we found that a stoichiometry of three high-affinity sites and one low-affinity site yielded a slightly better but not statistically significant ($p > 0.2$, paired Student's t-test) fit than the 2:2 stoichiometry (RMS = 0.31 ± 0.2 versus 0.37 ± 0.6 (mean ± SE, respectively). Table 1 lists the k_{on} and K_d values of CB_{28k} as derived from the heterogeneous binding site model for both stoichiometries.

DISCUSSION

We have used UV laser flash photolysis of DM-n in combination with model fitting to study the kinetic Ca^{2+} binding properties of human recombinant CB_{28k}. Our results demonstrate that CB_{28k} binds Ca^{2+} in at least two distinct kinetic patterns, one arising from high-affinity sites that bind Ca^{2+} with a k_{on} comparable to that of EGTA (i.e., $\sim 1 \times 10^7\ M^{-1}\ s^{-1}$) and another with lower affinity and an approximately eightfold faster k_{on}.

UV flash photolysis provides a means for eliciting rapid and large [Ca^{2+}] changes and deriving Ca^{2+} binding rate constants of Ca^{2+} buffers from nonlinear model analysis. The model explicitly included all Ca^{2+} binding reactions; parameters other than the unknown Ca^{2+} buffering rate constants were either measured or set at published values. Furthermore, the analysis avoided linearizing assumptions required for fitting analytical functions to the data (Neher, 1998a). As a consequence, robust signals with excellent signal-to-noise ratio generated in response to the large Ca^{2+} driving functions could be used to analyze the kinetic reactions. The use of UV flashes of varying energy allowed us to generate a range of $\Delta F/F$ transients and to fit the model predictions simultaneously. These constraints increase our confidence in the uniqueness of the derived kinetic parameters.

The brief dead time of the methodology makes it possible to faithfully resolve the rising phase of the fluorescence transient and thus obtain its amplitude directly rather than by extrapolating to critical early time points. By titrating the pre-flash [Ca^{2+}] to 1.5 μM, >99.5% of the DM-n was loaded with Ca^{2+}. Thus there is practically no rebinding of Ca^{2+} to DM-n regardless of UV flash energy, and photolysis produced steplike increases in [Ca^{2+}] in the absence of buffers (Fig. 2). In the presence of synthetic buffers or CBPs, any fluorescence decay can be solely ascribed to their Ca^{2+} binding properties (Figs. 3 *B*, 4, and 5).

As a test for this approach to estimating kinetic parameters of Ca^{2+} buffers, we determined the K_d and k_{on} of Ca^{2+} binding to EGTA. The model-derived K_d (71 ± 4 nM, n = 5) was in close agreement with those calculated from Scatchard analysis (68 ± 3.5 nM, n = 3, Fig. 3 *A*) and by the MaxChelator software. At pH 7.3, our k_{on} value of $1.05 \times 10^7\ M^{-1}\ s^{-1}$ matches that previously determined by stopped-flow analysis at the same pH (Smith et al., 1984), which is approximately fivefold faster than at pH 7.0 (Naraghi, 1997). Moreover, our K_d value of 71 nM is approximately fivefold lower than those reported at pH 7 (Harrison and Bers, 1987). Altogether, these results reinforce the notion that the higher affinity of EGTA at a lowered protonation state is due primarily to an increase in k_{on}, leaving k_{off} unchanged (Hellam and Podolsky, 1969; Tsien, 1980; Smith et al., 1984; Harrison and Bers, 1987).

The EGTA experiments demonstrate that our flash photolysis kinetic method is sufficiently sensitive to accurately resolve a K_d of less than 100 nM, even though 95% of EGTA is Ca^{2+} bound when 1.5 μM of [Ca^{2+}] is present before flash delivery. Thus, we chose to determine the K_d values of CB_{28k} from the analysis of flash photolysis transients, rather than from Scatchard analysis, to avoid the latter method's intrinsic difficulties in resolving K_d values of Ca^{2+}-binding sites that differ by less than an order of magnitude. No less problematic was the limited availability of the protein, given the substantial quantities that would be consumed by decalcification and titration of the protein sample (Celio et al., 1996). We used a KCl-based buffer solution with pH and osmolarity values intended to mimic the physiological intracellular conditions of mammalian CNS neurons. Given that Ca^{2+} binding to a buffer is usually associated with the release of protons (Tsien, 1980), the pH of the flash solutions was strongly buffered. For this study we excluded any Mg^{2+} from the solutions to avoid complications caused by UV flash-induced release of Mg^{2+} from DM-n (Kaplan and Ellis-Davies, 1988; Ayer and Zucker, 1999). It is known that the Ca^{2+} binding properties of certain EF-hand CBPs are influenced by [Mg^{2+}] because of binding competition between Ca^{2+} and Mg^{2+} for so-called mixed binding sites (Celio et al., 1996). Therefore, our results may provide upper limits for the apparent k_{on} and the affinity of CB_{28k} for Ca^{2+}, because it is possible that these parameters are lowered in the presence of physiological [Mg^{2+}].

Even though CB_{28k} binds four Ca^{2+} ions with domains that are characterized by stereotypical EF hand structural motifs (Celio et al., 1996), the ability of the heterogeneous binding sites model to drastically improve on the uniform binding sites model (Fig. 5 and Table 1) strongly argues for the existence of at least two types of kinetically distinct Ca^{2+}-binding sites on the protein, which is consistent with previous observations (Gross et al., 1987, 1988, 1993). The CB_{28k} model analysis contrasts sharply with the EGTA findings, which demonstrated that the experimental transients could be fitted well by a single (i.e., uniform) binding site model. Indeed, incorporation of a second, different site into the model for EGTA did not improve the RMS value of the fit (RMS values 0.205 versus 0.197, respectively; data not shown), whereas the need for adopting a heterogeneous model was evident. The correct stoichiometry of the two kinetically distinct Ca^{2+}-binding sites remains uncertain. The data could be fitted well, assuming a 2:2 or a 3:1

stoichiometry for the high- and low-affinity sites, respectively. It is important to note that the use of conventional techniques, such as stopped flow, would have likely made it impossible to resolve the rate constant associated with the fast Ca^{2+} binding site, because the fast fluorescence decay occurred within less than 2 ms (Fig. 5).

No attempt was made to characterize possible Ca^{2+}-dependent cooperative interactions between the binding sites, which have been reported for CB_{9k} (Linse and Chazin, 1995). Future studies of mutant CB_{28k} proteins with altered EF hand motifs should allow us to examine the Ca^{2+} binding properties of individual binding sites and clarify these important subtleties. Also, a number of technical advances should be incorporated to probe more sophisticated Ca^{2+} binding models. A faster equilibrating Ca^{2+} indicator dye would improve the accuracy of the derived kinetic parameters of the Ca^{2+} buffer under study because it would render the model analysis less sensitive to the precise rate constants of the dye. We believe that the recently introduced Fluo-5N (Molecular Probes) is a good candidate. In addition, it is desirable for the uncaging compound to have a reduced affinity for Mg^{2+}, which would make it possible to study the Ca^{2+} binding kinetics in the presence of physiological [Mg^{2+}]. An elevated affinity for Ca^{2+} would permit the generation of Ca^{2+} steps at lower, more physiological [Ca^{2+}]. This may also allow us to resolve higher affinity sites in CBPs, such as the 1 nM one reported by Gross et al. (1993), which remained undetectable by our current method. The novel caged Ca^{2+} compound dimethoxynitrophenyl-EGTA-4 (DMNPE-4) was reported to have a very low affinity for Mg^{2+}, but unfortunately it has an even lower affinity for Ca^{2+} than does DM-n (DelPrincipe et al., 1999).

APPENDIX: KINETIC MODEL FOR FLASH PHOTOLYSIS OF DM-n AND DETECTION BY Ca^{2+} INDICATORS

Definition of terms

The model schematized in Fig. 1 was modified from Escobar et al. (1997). Note that nonsubscripted concentrations are functions of time (e.g., $[Ca^{2+}] = [Ca^{2+}(t)]$. The time notation has been omitted for readability. The values for the subscripted concentrations and kinetic parameters were adopted from the published literature or our own measurements (indicated in parentheses).

$[Ca^{2+}]$	free calcium concentration
$[Ca^{2+}]_{t=0}$	resting (initial) free calcium concentration = 1.5 μM (measured)
$[Ca^{2+}]_T$	total calcium concentration
$[DM]_T$	total concentration of DM-n = 5 mM
[DM]	concentration of free DM-n
α	fraction of DM-n photolysed by a flash = fit parameter
[DM1]	concentration of free DM-n complex to be photolyzed
[DM2]	concentration of free DM-n complex **not** photolyzed
[CaDM1]	concentration of Ca^{2+}-DM-n complex to be photolyzed
[CaDM2]	concentration of Ca^{2+}-DM-n complex **not** photolyzed
$k_{on\text{-}DM}$	binding rate constant of DM-n = 0.03 μM^{-1} ms^{-1} (Escobar et al., 1997)
$k_{off\text{-}DM}$	dissociation rate constant of DM-n = 0.00006 ms^{-1} (derived from K_d)
K_{DM}	equilibrium dissociation constant of DM-n = $k_{off\text{-}DM}/k_{on\text{-}DM}$ = 2 nM (measured)
$k^*_{off\text{-}DM}$	dissociation rate constant of DM-n after photolysis = 75 ms^{-1} (Kaplan and Ellis-Davies, 1988)
$\tau_{photolysis}$	time constant of photolysis reaction = 20 μs (Kaplan and Ellis-Davies, 1988)
$[D]_T$	total Ca^{2+} indicator dye concentration = 100 μM
[D]	concentration of free Ca^{2+} indicator dye
[CaD]	concentration of Ca^{2+}-dye complex
K_{d-D}	equilibrium constant of OGB-5N = 45 μM (measured)
$k_{off\text{-}D}$	dissociation rate constant of OGB-5N (ms^{-1}) = 5.6 ms^{-1}) = 5.6 ms^{-1} (DiGregorio et al., 1999)
k_{on-D}	binding rate constant of OGB-5N = 0.124 μM^{-1} ms^{-1} (derived from K_d)
F_{ratio}	ratio of F_{max} over F_{min} = 30.8 (measured)
t_{pulse}	point (in time) of flash pulse delivery
$[B_i]_T$	total *i*th buffer concentration = known
$[B_i]$	concentration of *i*th free buffer
$[CaB_i]$	concentration of *i*th Ca^{2+}-buffer complex
k_{on-Bi}	binding rate constant (on) of *i*th buffer (μM^{-1} ms^{-1}) = fit parameter
k_{off-Bi}	dissociation rate constant (off) of *i*th buffer (ms^{-1}) = fit parameter

The model

DM-n, the Ca^{2+} indicator dye, and buffers 1 and 2 obey simple bimolecular binding kinetic reaction schemes.

Flash photolysis assumptions

1. The total DM-n concentration $[DM]_T$ is divided into a photolyzable fraction $[DM1]_T$ and a nonphotolyzable fraction $[DM2]_T$.

2. The flash energy (α) determines the proportion of the photolyzable fraction,

$$[DM1]_T = \alpha[DM]_T \tag{1}$$

3. The kinetic reaction scheme for fraction 1 *before* the flash is

$$[Ca^{2+}] + [DM1] \underset{k_{off-DM}}{\overset{k_{on-DM}}{\rightleftharpoons}} [CaDM1] \tag{2}$$

4. The kinetic reaction scheme for fraction 1 *after* the flash is

$$[Ca^{2+}] + [DM1] \underset{k^*_{off-DM}}{\overset{k_{on-DM}}{\rightleftharpoons}} [CaDM1] \tag{2'}$$

5. The kinetic reaction scheme for fraction 2 before and after the flash is

$$[Ca^{2+}] + [DM2] \underset{k_{off-DM}}{\overset{k_{on-DM}}{\rightleftharpoons}} [CaDM2] \tag{3}$$

6. After t_{pulse}, the photolysis reaction proceeds with a transitional dissociation rate constant, k_{trans}, given by

$$k_{trans} = k_{off-DM} + (k^*_{off-DM} - k_{off-DM}) \times \left[1 - \exp\frac{-(t - t_{pulse})}{\tau_{photolysis}}\right] \tag{4}$$

Ca^{2+} indicator kinetic scheme

$$[Ca^{2+}] + [D] \underset{k_{off-D}}{\overset{k_{on-D}}{\rightleftharpoons}} [CaD] \quad (5a)$$

Ca^{2+} buffer kinetic scheme

$$[Ca^{2+}] + [B_i] \underset{k_{off-B_i}}{\overset{k_{on-B_i}}{\rightleftharpoons}} [CaB_i] \quad (5b)$$

Differential equations

DM-n before the flash

$$\frac{d[CaDM1]}{dt} = k_{on-DM} \times [Ca^{2+}] \times [DM1] - k_{off-DM} \times [CaDM1] \quad (6)$$

$$\frac{d[CaDM2]}{dt} = k_{on-DM} \times [Ca^{2+}] \times [DM2] - k_{off-DM} \times [CaDM2] \quad (7)$$

DM-n after the flash

$$\frac{d[CaDM1]}{dt} = k_{on-DM} \times [Ca^{2+}] \times [DM1] - k_{trans} \times [CaDM1] \quad (8)$$

Calcium indicator

$$\frac{d[CaD]}{dt} = k_{on-D} \times [Ca^{2+}] \times [D] - k_{off-D} \times [CaD] \quad (9)$$

Calcium buffers

$$\frac{d[CaD]}{dt} = k_{on-D} \times [Ca^{2+}] \times [B_i] - k_{off-D} \times [CaD] \quad (10)$$

Conservation equations

DM-nitrophen

$$[DM]_T = [DM1]_T + [DM2]_T \quad (11)$$

$$[DM1]_T = [DM1] + [CaDM1] \quad (12)$$

$$[DM2]_T = [DM2] + [CaDM2] \quad (13)$$

Calcium dye, buffers, and calcium

$$[D]_T = [D] + [CaD] \quad (14)$$

$$[B_i]_T = [B_i] + [CaB_i] \quad (15)$$

$$[Ca^{2+}]_T = [CaD] + [CaDM1] + [CaDM2] + \sum[CaB_i] + [Ca^{2+}] \quad (16)$$

Initial conditions

$$[Ca^{2+}] = [Ca^{2+}]_{t=0} \quad (17)$$

$$[CaD] = \frac{[Ca]_{t=0} \times [D]_T}{k_{off-D}/k_{on-D} + [Ca]_{t=0}} \quad (18)$$

$$[CaB_i] = \frac{[Ca]_{t=0} \times [B_i]_T}{k_{off-B_i}/k_{on-B_i} + [Ca]_{t=0}} \quad (19)$$

$$[DM1] = [DM]_T \times \alpha - - - [CaDM1] \quad (20)$$

$$[CaDM1] = \frac{[Ca^{2+}]_{t=0} \times [DM]_T \times \alpha}{(k_{off-DM}/k_{on-DM} + [Ca^{2+}]_{t=0})} \quad (21)$$

$$[DM2] = [DM]_T \times (1 - \alpha) - [CaM2] \quad (22)$$

$$[CaDM2] = \frac{[Ca^{2+}]_{t=0} \times [DM]_T \times (1 - \alpha)}{(k_{off-DM}/k_{on-DM} + [Ca^{2+}]_{t=0})} \quad (23)$$

Model output

$$\frac{\Delta F}{F} = \frac{\Delta F(t)}{F_{rest}} = \frac{[CaD] \times (F_{ratio} - 1) + [D]_T}{[CaD]_{t=0} \times (F_{ratio} - 1) + [D]_T} - 1 \quad (24)$$

Numerical integration method

The numerical integration method was the fourth-order Runge-Kutta method (Berkeley Madonna 8.0).

The authors are grateful to Dr. K. G. Baimbridge (University of British Columbia, Vancouver, BC, Canada) for generously supplying human recombinant calbindin-D_{28k}. We also thank Drs. M. DiFranco, D. DiGregorio, J. R. Monck, and Z. Nusser for helpful comments on the manuscript.

UVN was supported by an American Epilepsy Foundation predoctoral fellowship. Additional support was provided by the National Institutes of Health, National Institute of Neurological Disorders and Stroke (grant NS 27528-07) and the Coelho Endowment to IM, and the National Institutes of Health, National Institute of Arthritis and Musculoskeletal and Skin Diseases (grant AR 25201) to JLV.

REFERENCES

Adler, E. M., G. J. Augustine, S. N. Duffy, and M. P. Charlton. 1991. Alien intracellular calcium chelators attenuate neurotransmitter release at the squid giant synapse. *J. Neurosci.* 11:1496–1507.

Airaksinen, M. S., J. Eilers, O. Garaschuk, H. Thoenen, A. Konnerth, and M. Meyer. 1997. Ataxia and altered dendritic calcium signaling in mice carrying a targeted null mutation of the calbindin D28k gene. *Proc. Natl. Acad. Sci. USA.* 94:1488–1493.

Atluri, P. P., and W. G. Regehr. 1996. Determinants of the time course of facilitation at the granule cell to Purkinje cell synapse. *J. Neurosci.* 16:5661–5671.

Ayer, R. K., Jr., and R. S. Zucker. 1999. Magnesium binding to DM-nitrophen and its effect on the photorelease of calcium. *Biophys. J.* 77:3384–3393.

Baimbridge, K. G. 1992. Calcium-binding proteins in the dentate gyrus. *Epilepsy Res. Suppl.* 7:211–220.

Baudet, S., L. Hove-Madsen, and D. M. Bers. 1994. How to make and use calcium-specific mini- and microelectrodes. *Methods Cell Biol.* 40: 93–113.

Bayley, P., P. Ahlstrom, S. R. Martin, and S. Forsen. 1984. The kinetics of calcium binding to calmodulin: Quin 2 and ANS stopped-flow fluorescence studies. *Biochem. Biophys. Res. Commun.* 120:185–191.

Bers, D. M. 1982. A simple method for the accurate determination of free [Ca] in Ca-EGTA solutions. *Am. J. Physiol.* 242:C404–C408.

Bers, D. M., C. W. Patton, and R. Nuccitelli. 1994. A practical guide to the preparation of Ca^{2+} buffers. *Methods Cell Biol.* 40:3–29.

Celio, M. R. 1990. Calbindin D-28k and parvalbumin in the rat nervous system. *Neuroscience.* 35:375–475.

Celio, M. R., T. L. Pauls, and B. Schwaller. 1996. Guidebook to the Calcium-Binding Proteins. Sambrook & Tooze Publications at Oxford University Press, Oxford and New York.

Chen, C., and W. G. Regehr. 1999. Contributions of residual calcium to fast synaptic transmission. *J. Neurosci.* 19:6257–6266.

Cheung, W. T., D. E. Richards, and J. H. Rogers. 1993. Calcium binding by chick calretinin and rat calbindin D28k synthesised in bacteria. *Eur. J. Biochem.* 215:401–410.

Czerlinski, G. H. 1966. Chemical Relaxation: An Introduction to Theory and Application of Stepwise Perturbation. M. Dekker, New York.

Davis, A. F., J. Bai, D. Fasshauer, M. J. Wolowick, J. L. Lewis, and E. R. Chapman. 1999. Kinetics of synaptotagmin responses to Ca^{2+} and assembly with the core SNARE complex onto membranes *Neuron.* 24:363–376 (erratum 24:1049).

Davis, T. N. 1992. What's new with calcium? *Cell.* 71:557–564.

DelPrincipe, F., M. Egger, G. C. Ellis-Davies, and E. Niggli. 1999. Two-photon and UV-laser flash photolysis of the Ca^{2+} cage, dimethoxynitrophenyl-EGTA-4. *Cell Calcium.* 25:85–91.

DiGregorio, D. A., J. Marengo, A. Peskoff, and J. L. Vergara. 1998. Measurement of presynaptic calcium microdomains in a cultured neuromuscular junction. *In Meeting for the Society of Neuroscience.* D-72.

DiGregorio, D. A., A. Peskoff, and J. L. Vergara. 1999. Measurement of action potential-induced presynaptic calcium domains at a cultured neuromuscular junction. *J. Neurosci.* 19:7846–7859.

DiGregorio, D. A., and J. L. Vergara. 1997. Localized detection of action potential-induced presynaptic calcium transients at a *Xenopus* neuromuscular junction. *J. Physiol. (Lond.).* 505:585–592.

DiPolo, R., H. Rojas, J. Vergara, R. Lopez, and C. Caputo. 1983. Measurements of intracellular ionized calcium in squid giant axons using calcium-selective electrodes. *Biochim. Biophys. Acta.* 728:311–318.

Eigen, M. 1963. Fast elementary steps in chemical reaction mechanisms. *Pure Appl. Chem.* 6:97–115.

Ellis-Davies, G. C., and J. H. Kaplan. 1994. Nitrophenyl-EGTA, a photolabile chelator that selectively binds Ca^{2+} with high affinity and releases it rapidly upon photolysis. *Proc. Natl. Acad. Sci. USA.* 91:187–191.

Escobar, A. L., F. Cifuentes, and J. L. Vergara. 1995. Detection of Ca(2+)-transients elicited by flash photolysis of DM-nitrophen with a fast calcium indicator. *FEBS Lett.* 364:335–338.

Escobar, A. L., P. Velez, A. M. Kim, F. Cifuentes, M. Fill, and J. L. Vergara. 1997. Kinetic properties of DM-nitrophen and calcium indicators: rapid transient response to flash photolysis. *Pflugers Arch.* 434:615–631.

Fierro, L., and I. Llano. 1996. High endogenous calcium buffering in Purkinje cells from rat cerebellar slices. *J. Physiol. (Lond.).* 496: 617–625.

Gross, M. D., M. Gosnell, A. Tsarbopoulos, and W. Hunziker. 1993. A functional and degenerate pair of EF hands contains the very high affinity calcium-binding site of calbindin-D28K. *J. Biol. Chem.* 268: 20917–20922.

Gross, M. D., R. Kumar, and W. Hunziker. 1988. Expression in *Escherichia coli* of full-length and mutant rat brain calbindin D28. Comparison with the purified native protein. *J. Biol. Chem.* 263:14426–14432.

Gross, M. D., G. L. Nelsestuen, and R. Kumar. 1987. Observations on the binding of lanthanides and calcium to vitamin D-dependent chick intestinal calcium-binding protein. Implications regarding calcium-binding protein function. *J. Biol. Chem.* 262:6539–6545.

Harrison, S. M., and D. M. Bers. 1987. The effect of temperature and ionic strength on the apparent Ca affinity of EGTA and the analogous Ca chelators BAPTA and dibromo-BAPTA. *Biochim. Biophys. Acta.* 925: 133–143.

Hellam, D. C., and R. J. Podolsky. 1969. Force measurements in skinned muscle fibres. *J. Physiol. (Lond.).* 200:807–819.

Hollingworth, S., M. Zhao, and S. M. Baylor. 1996. The amplitude and time course of the myoplasmic free [Ca^{2+}] transient in fast-twitch fibers of mouse muscle. *J. Gen. Physiol.* 108:455–469.

Kao, J. P., and R. Y. Tsien. 1988. Ca^{2+} binding kinetics of fura-2 and azo-1 from temperature-jump relaxation measurements. *Biophys. J.* 53: 635–639.

Kaplan, J. H., and G. C. Ellis-Davies. 1988. Photolabile chelators for the rapid photorelease of divalent cations. *Proc. Natl. Acad. Sci. USA.* 85:6571–6575.

Kawasaki, H., S. Nakayama, and R. H. Kretsinger. 1998. Classification and evolution of EF-hand proteins. *Biometals.* 11:277–295.

Kennedy, M. B. 1989. Regulation of neuronal function by calcium. *Trends Neurosci.* 12:417–420.

Klapstein, G. J., S. Vietla, D. N. Lieberman, P. A. Gray, M. S. Airaksinen, H. Thoenen, M. Meyer, and I. Mody. 1998. Calbindin-D28k fails to protect hippocampal neurons against ischemia in spite of its cytoplasmic calcium buffering properties: evidence from calbindin-D28k knockout mice. *Neuroscience.* 85:361–373.

Linse, S., and W. J. Chazin. 1995. Quantitative measurements of the cooperativity in an EF-hand protein with sequential calcium binding. *Protein Sci.* 4:1038–1044.

Martin, S. R., S. Linse, C. Johansson, P. M. Bayley, and S. Forsen. 1990. Protein surface charges and Ca^{2+} binding to individual sites in calbindin D9k: stopped-flow studies. *Biochemistry.* 29:4188–4193.

McGuigan, J. A., D. Luthi, and A. Buri. 1991. Calcium buffer solutions and how to make them: a do it yourself guide. *Can. J. Physiol. Pharmacol.* 69:1733–1749.

Nägerl, U. V., I. Mody, M. Jeub, A. A. Lie, C. E. Elger, and H. Beck. 2000. Surviving granule cells of the sclerotic human hippocampus have reduced Ca(2+) influx because of a loss of calbindin-D(28k) in temporal lobe epilepsy. *J. Neurosci.* 20:1831–1836.

Naraghi, M. 1997. T-jump study of calcium binding kinetics of calcium chelators. *Cell Calcium.* 22:255–268.

Neher, E. 1998a. Usefulness and limitations of linear approximations to the understanding of Ca^{++} signals *Cell Calcium.* 24:345–357 (erratum 25:275).

Neher, E. 1998b. Vesicle pools and Ca^{2+} microdomains: new tools for understanding their roles in neurotransmitter release. *Neuron.* 20: 389–399.

Pasti, L., G. Carmignoto, T. Pozzan, R. Battini, S. Ferrari, G. Lally, and P. C. Emson. 1999. Cellular calcium handling in brain slices from calbindin D28k-deficient mice. *Neuroreport.* 10:2367–2372.

Smith, P. D., G. W. Liesegang, R. L. Berger, G. Czerlinski, and R. J. Podolsky. 1984. A stopped-flow investigation of calcium ion binding by ethylene glycol bis(beta-aminoethyl ether)-*N*,*N*′-tetraacetic acid. *Anal. Biochem.* 143:188–195.

Stern, M. D. 1992. Buffering of calcium in the vicinity of a channel pore. *Cell Calcium.* 13:183–192.

Tsien, R. Y. 1980. New calcium indicators and buffers with high selectivity against magnesium and protons: design, synthesis, and properties of prototype structures. *Biochemistry.* 19:2396–2404.

Veenstra, T. D., K. L. Johnson, A. J. Tomlinson, S. Naylor, and R. Kumar. 1997. Determination of calcium-binding sites in rat brain calbindin D28K by electrospray ionization mass spectrometry. *Biochemistry.* 36: 3535–3542.

Vergara, J., and M. Delay. 1985. The use of metallochromic Ca indicators in skeletal muscle. *Cell Calcium.* 6:119–132.

Vergara, J., and M. DiFranco. 1992. Imaging of calcium transients during excitation-contraction coupling in skeletal muscle fibers. *Adv. Exp. Med. Biol.* 311:227–236.